

## Article

# Modelling and Design of a Novel Integrated Heat Exchange Reactor for Oxy-Fuel Combustion Flue Gas Deoxygenation

Hongtian Ge<sup>1</sup>, Andrew J. Furlong<sup>2</sup> , Scott Champagne<sup>3,\*</sup>, Robin W. Hughes<sup>3</sup>, Jan B. Haelssig<sup>1</sup> and Arturo Macchi<sup>1,\*</sup> 

<sup>1</sup> Department of Chemical and Biological Engineering, University of Ottawa, 161 Louis Pasteur Street, Ottawa, ON K1N 6N5, Canada; rge006@uottawa.ca (H.G.); jhaelssi@uottawa.ca (J.B.H.)

<sup>2</sup> Department of Process Engineering and Applied Science, Dalhousie University, Halifax, NS B3H 4R2, Canada; afurlong@dal.ca

<sup>3</sup> Natural Resources Canada, CanmetENERGY, 1 Haanel Drive, Ottawa, ON K1A 1M1, Canada; robin.hughes@nrcan-rncan.gc.ca

\* Correspondence: scott.champagne@nrcan-rncan.gc.ca (S.C.); arturo.macchi@uottawa.ca (A.M.)

**Abstract:** The concentration of residual O<sub>2</sub> in oxy-fuel combustion flue gas needs to be reduced before CO<sub>2</sub> transportation, utilization, or storage. An original application of the printed circuit heat exchanger (PCHE) for catalytic combustion with natural gas (catalytic deoxygenation) is described for reducing the residual O<sub>2</sub> concentration. The PCHE design features multiple adiabatic packed beds with interstage cooling and fuel injection, allowing precise control over the reaction extent and temperature within each reaction stage through the manipulation of fuel and utility flow rates. This work describes the design of a PCHE for methane–oxygen catalytic combustion where the catalyst loading is minimized while reducing the O<sub>2</sub> concentration from 3 vol% to 100 ppmv, considering a maximum adiabatic temperature rise of 50 °C per stage. Each PCHE design differs by the number of reaction stages and its individual bed lengths. As part of the design process, a one-dimensional transient reduced-order reactor model (1D ROM) was developed and compared to temperature and species concentration axial profiles from 3D CFD simulations. The final design consists of five reaction stages and four heat exchanger sections, providing a PCHE length of 1.09 m at a processing rate of 12.3 kg/s flue gas per m<sup>3</sup> PCHE.

**Keywords:** flue gas processing; catalytic deoxygenation; process intensification; printed circuit heat exchanger; transient model



**Citation:** Ge, H.; Furlong, A.J.; Champagne, S.; Hughes, R.W.; Haelssig, J.B.; Macchi, A. Modelling and Design of a Novel Integrated Heat Exchange Reactor for Oxy-Fuel Combustion Flue Gas Deoxygenation. *Energies* **2024**, *17*, 1474. <https://doi.org/10.3390/en17061474>

Academic Editor: Bohung Kim

Received: 12 February 2024

Revised: 8 March 2024

Accepted: 15 March 2024

Published: 19 March 2024



**Copyright:** © 2024 by the authors. Licensee MDPI, Basel, Switzerland. This article is an open access article distributed under the terms and conditions of the Creative Commons Attribution (CC BY) license (<https://creativecommons.org/licenses/by/4.0/>).

## 1. Introduction

Rising climate change and environmental concerns require a reduction in anthropogenic carbon dioxide emissions. One part of the emission reduction solution is carbon capture utilization and storage (CCUS). Conventional air–fuel combustion flue gases contain 9 to 15 vol% of CO<sub>2</sub>, with the balance being primarily nitrogen. Separating CO<sub>2</sub> from nitrogen in flue gas after combustion is an energy-intensive process [1]. Oxy-fuel combustion is an attractive alternative as it replaces air with high-purity (typically > 95 vol%) oxygen, yielding a flue gas with a dry-basis CO<sub>2</sub> and O<sub>2</sub> content of around 96 and 3 vol%, respectively [2,3]. The high concentration of CO<sub>2</sub> reduces the steps required to process the CO<sub>2</sub> for transportation and storage. Impurities such as SO<sub>x</sub> and NO<sub>x</sub> can be removed through oxidation with the O<sub>2</sub> already present in the flue gas, followed by scrubbing to produce dilute sulfuric acid and nitric acid, respectively [2]. The remaining major impurity is residual O<sub>2</sub>, which is limited to very low concentrations (<100 ppmv) in pipelines, sequestration sites, and utilization processes [4]. Oxy-fuel technologies will require an oxygen removal unit in order for the CO<sub>2</sub> product to meet this stringent specification.

Catalytic combustion with natural gas is a promising method to remove residual O<sub>2</sub>, which is hereby referred to as catalytic deoxygenation. Commercial catalytic packed

bed reactors with integrated cooling typically have coolant flowing through tube bundles embedded in the reactor [5]. Another configuration uses a shell-and-tube heat exchanger, where the tubes are packed with a catalyst and the coolant flows in the shell [6]. Heat management in both cases can be challenging as a single stream of cooling fluid is used throughout the entire reactor. One method for improving temperature control is to use multiple adiabatic packed beds with distributed fuel injection and interstage cooling [6]. A further improvement in controllability and performance can be achieved by incorporating the intensified transport rates found in the Marbond™ heat exchanger from Chart Marston and the printed circuit heat exchanger (PCHE) from Heatric [7,8]. PCHEs have many desirable qualities, such as (1) a high operating temperature of up to 980 °C; (2) high pressure capabilities of up to 965 bar; (3) a high surface area density at high pressures (1300 m<sup>2</sup>/m<sup>3</sup> at 100 bar); (4) a minimum approach temperature as low as 1 °C; and (5) a high heat exchanger effectiveness of up to 99% [8,9]. Due to these desirable qualities, PCHEs have been designed for applications such as N<sub>2</sub>- and supercritical CO<sub>2</sub>-based Brayton cycles, steam generation for small modular reactors, and waste heat recovery from exhaust gas [10–13]. However, the PCHE design as a process-intensified reactor unit can be further explored.

A catalytic deoxygenation unit is designed as multiple adiabatic packed bed reactors with interstage printed circuit heat exchange and fuel injection. Similar approaches have been used for steam–methane reforming and Fischer–Tropsch processes [8,14,15]. The design utilizes chemically etched plates for the flow of process, fuel, and utility fluids in between packed bed reactor sections. The entire assembly is diffusion-bonded to fuse the plates into a PCHE (see Figure 1 [14]).

In the context of using a PCHE for the catalytic deoxygenation of oxy-fuel flue gas, interstage cooling can recover high-quality heat from the reaction mixture. Variations in flue gas flow can also be better managed when the utility fluid flow rate is adjusted to counteract inlet temperature deviations, and O<sub>2</sub> composition deviations are countered by adjusting the fuel flow rate. The reactor design can also be adjusted for higher O<sub>2</sub> concentrations by adding extra beds, and the reactor can easily be scaled to accommodate higher throughputs.

The rectangular slots in the path of the process fluid flow shown in Figure 1 represent the space allocated for catalyst packing. The green and blue slots at the top and bottom of the plates are to distribute fuel and utility fluid (connected to the respective headers), respectively. The flue gas, or more generically, the process fluid, alternates between reaction in a packed bed reaction stage and crossflow heat exchange with utility fluid in a heat exchanger section. Fuel is injected directly into the inlet of a packed stage using the fuel distribution plate. Alternating reactor and heat exchange sections allow the reactor to operate near the maximum applicable temperature of the reaction for fast kinetics and the recovery of the highest possible quality heat. A configuration of four plates in the order of process, fuel, process, and utility forms one repeating unit, to be enclosed by another utility fluid plate above the top process fluid plate for the simplest form of a complete PCHE. This plate design allows for freedom in scalability, where the throughput of the PCHE can be increased by stacking more repeating units.

Considering the above, the objective of this work is to design a novel PCHE for the catalytic deoxygenation of oxy-fuel combustion flue gas. First, a one-dimensional transient reduced-order reactor model (1D ROM) is developed and compared to three-dimensional computational fluid dynamic simulations to ensure consistency. Afterwards, the 1D ROM is used to design the reaction stages, along with a thermal circuit approach to design the heat exchange sections. The reaction stages and heat exchange sections combine to form the full PCHE reactor design.

The design intent of the reaction stages is to reduce the O<sub>2</sub> content of the flue gas from 3 vol% to ≤100 ppmv to meet pipeline or other transportation, utilization, or storage specifications. The heat of combustion is recovered by superheating saturated steam from 181 °C to 231 °C and amounts to approximately 275 kJ per kg of treated flue gas. Further

heat recovery can be achieved by using the treated flue gas to pre-heat the inlet flue gas in a heat exchange section prior to the first reaction stage (see Figure 1b).

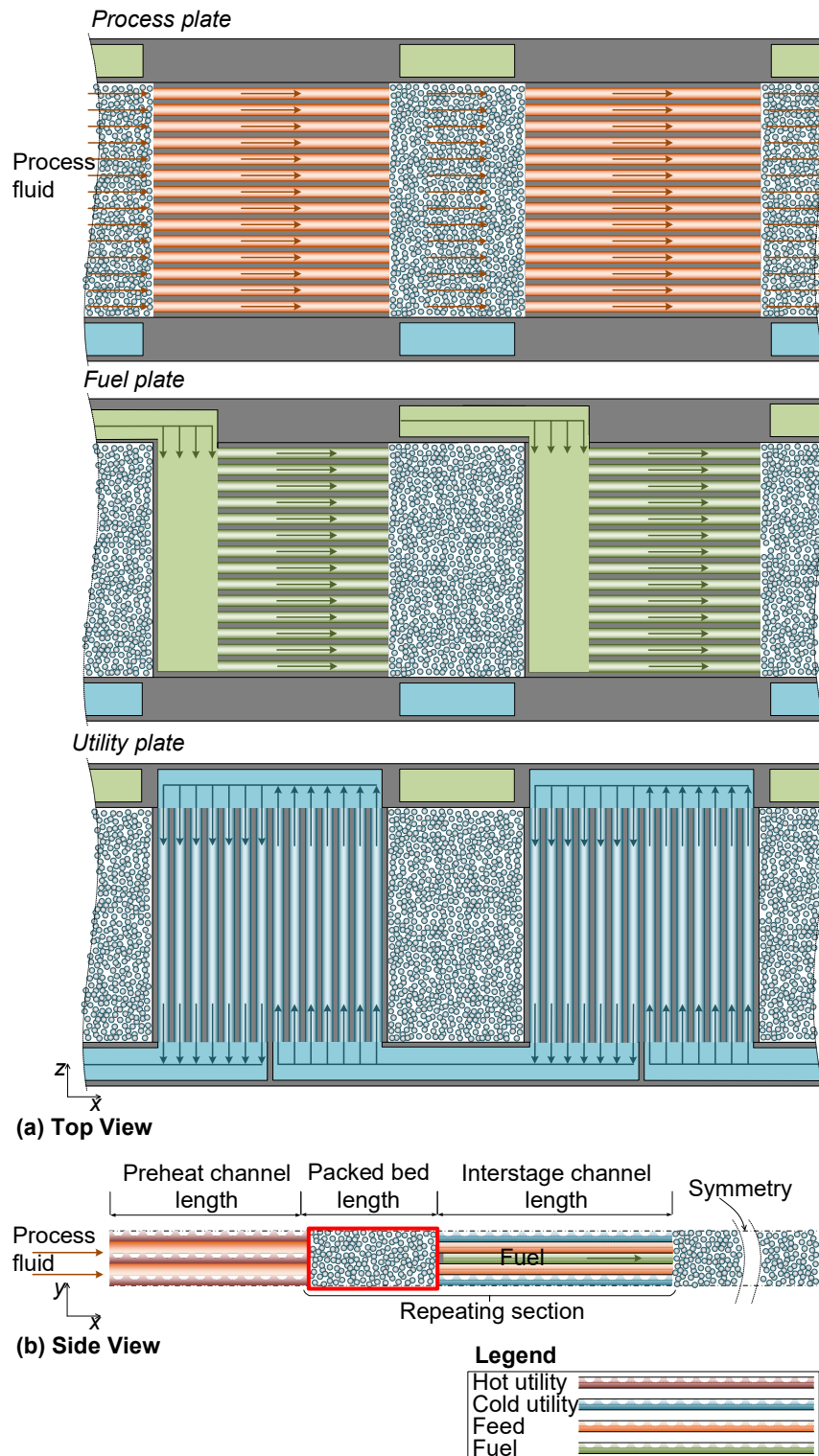


**Figure 1.** (a) Top view of PCHE plate design, where the plates from top to bottom are (1) process fluid flow, (2) fuel fluid distribution, and (3) utility fluid flow. Process fluid and fuel flows are co-current, whereas the utility fluid flows counter-current with a two-pass crossflow configuration. The number of utility fluid passes is adjusted to the heat transfer demand. (b) Side view of PCHE plate design shows alternating heat exchanger sections and adiabatic packed bed sections.

## 2. One-Dimensional Transient Reduced-Order Reactor Model

Figure 1b shows the modelled reaction stage enclosed in red. The symmetry in the  $y$ - and  $z$ -axes shown in Figure 1 allows for modelling one single repeating unit with sufficient width (e.g., two flow channels on the  $z$ -axis) to achieve the effect of modelling a complete packed bed.

### 2.1. Governing Equations

A one-dimensional flow is assumed for the reactor model considering that the inlet gas is evenly distributed into the packed bed by the process flow channels and the wall effects are marginal due to a relatively wide packed bed. The chemistry is solved using Cantera (version 2.5.1) [16], where all the gas- and solid-phase reaction rates as well as the enthalpies of the reactions are calculated. Only axial heat conduction is included for the packed bed, and radiation heat transfer is excluded due to the relatively low reaction temperature ( $\leq 550$  °C) for this PCHE design.

The 1D ROM is divided into the gas and solid phases, for which the species mass and energy conservation equations are solved. The reaction rate calculation in the solid phase can accommodate surface reactions with absorption/desorption steps and a site balance or simplified solid-phase reaction kinetics without a site balance. The Ergun equation is used to calculate the gas-phase pressure drop across the packed bed, assuming incompressible flow due to a maximum design pressure loss of 10%. All the governing equations are derived for the net direction of flow ( $x$ -axis).

Continuity:

$$\dot{m} = \rho_g u_g A_C \quad (1)$$

Momentum conservation:

$$-\frac{dP}{dx} = \left( \frac{150\mu_g (1-\epsilon)^2}{d_{sv}^2 \epsilon^3} u_g + \frac{1.75\rho_g (1-\epsilon)}{d_{sv}} \frac{u_g^2}{\epsilon^3} \right) \quad (2)$$

Energy conservation in the gas phase:

$$\frac{\partial(\rho_g H_g)}{\partial t} \epsilon = -\frac{\partial(u_g \rho_g H_g)}{\partial x} + h_g a_c (T_s - T_g) + q_{R,g} \quad (3)$$

Energy conservation in the solid phase:

$$\frac{\partial(\rho_s H_s)}{\partial t} (1-\epsilon) = (1-\epsilon) k_s \frac{\partial^2 T_s}{\partial x^2} + h_g a_c (T_g - T_s) + q_{R,s} \quad (4)$$

Species mass conservation in the gas phase:

$$\frac{\partial Y_g}{\partial t} = -\frac{\partial(u_g \rho_g Y_g)}{\epsilon \rho_g \partial x} + D_{eff} \frac{\partial^2(\rho_g Y_g)}{\rho_g \partial x^2} + k_m \frac{a_c}{\epsilon} (Y_s - Y_g) + R_g \quad (5)$$

Species mass conservation in the solid phase:

$$\frac{\partial Y_s}{\partial t} = k_m \frac{a_c}{1-\epsilon} (Y_g - Y_s) + R_s \quad (6)$$

The axial dispersion coefficient,  $D_{eff}$ , is determined using data provided by Levenspiel et al. [17]. The Gunn analogy [18] for both heat and mass transfer is used to calculate the interphase heat and mass transfer coefficients in Equations (7) and (8).

$$Nu = (7 - 10\epsilon + 5\epsilon^2) \times (1 + 0.7Re_p^{0.2}Pr^{\frac{1}{3}}) + (1.33 - 2.4\epsilon + 1.2\epsilon^2) \times Re_p^{0.7}Pr^{\frac{1}{3}} \quad (7)$$

$$Sh = Nu \left( \frac{Sc}{Pr} \right)^{\frac{1}{3}} \quad (8)$$

## 2.2. Solution Structure

The 1D ROM was programmed in Python and discretized into  $j$  equally sized volumes in the axial direction, according to Figure 2. All the governing equations are solved for each discretized volume at each time step,  $n$ , until the end of the specified solution time span, as per Figure 3. The numerical method uses a semi-implicit solution scheme for each time step; see Equations (9) and (10) for the explicit and semi-implicit time steps.

$$y_{t_{n+1}'} = y_{t_n} + f(y_{t_n}) \times dt \quad (9)$$

$$y_{t_{n+1}} = y_{t_n} + \frac{f(y_{t_n}) + f(y_{t_{n+1}'})}{2} \times dt \quad (10)$$

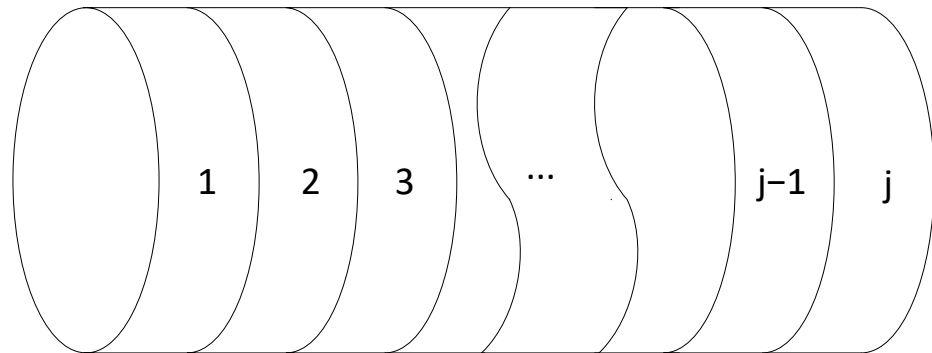


**Figure 2.** Spatial discretization of the 1D ROM.

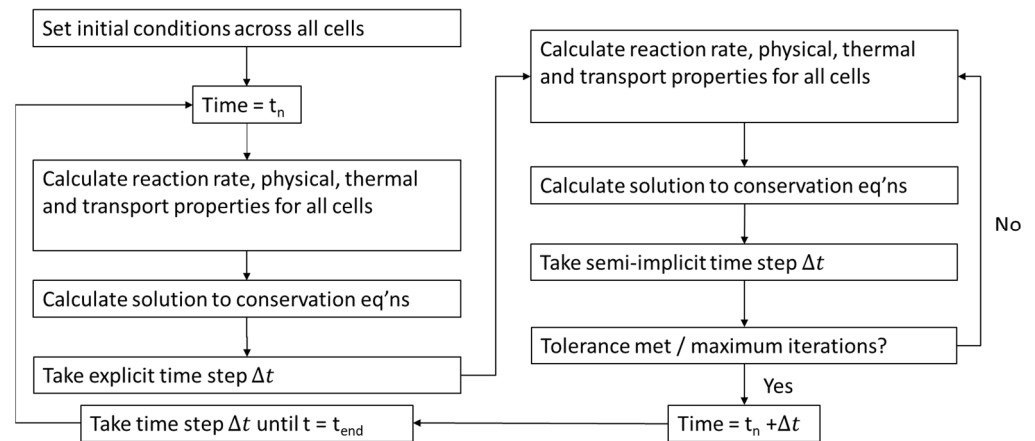


**Figure 3.** Transient solution scheme of the 1D ROM.

## 2.3. Reaction Kinetics

The methane oxidation kinetics on Pd/Co<sub>3</sub>O<sub>4</sub> are selected and presented in Table 1. The Arrhenius kinetic parameters are applicable from 250 to 550 °C in wet, lean environments with a methane concentration of 1000–5000 ppmv and a water vapour concentration of 0–5 vol% [19]. Moreover, the reaction kinetics are pseudo-first-order with respect to methane and applicable to reaction mixtures with O<sub>2</sub> concentrations as low as 0 vol% over a temperature range of 400–550 °C due to the oxygen supplying the ability of the Co<sub>3</sub>O<sub>4</sub> support [20].

**Table 1.** Arrhenius kinetic parameters for methane oxidation on Pd/Co<sub>3</sub>O<sub>4</sub> in wet, lean environments [19].

Parameter	Pre-Exponential Factor [L/(g·s)]	Activation Energy [J/mol]
Value	46,365	90,738

### 3. Design of the PCHE

#### 3.1. Process Constraints

The upper operating temperature is 550 °C for the selected reaction kinetic model, and this is also a reasonable temperature limit for stainless steel reactor construction. Furthermore, the temperature rise within a single reaction stage is limited to 50 °C to reduce thermal stress on the material of construction [6], which then results in temperatures between 500 and 550 °C for each reaction stage. The operating pressure is set to a maximum of 1000 kPa to ensure this design could be fabricated using conventional welding techniques, while the total pressure drop is limited to 10% considering compressor duty.

#### 3.2. Base Case Geometry and Operating Conditions

The process fluid channels and plate dimensions for the PCHE base design are shown in Figure 4. The process, utility, and fuel flow channels and plates share the same dimensions, with semi-circular channels being 3 mm in diameter, with a plate thickness of 3.5 mm and a 2 mm separation between the flow channels. Four channels are shown for illustration purposes, while the plate can be scaled in the z-direction to accommodate more channels for different total inlet flow rates.

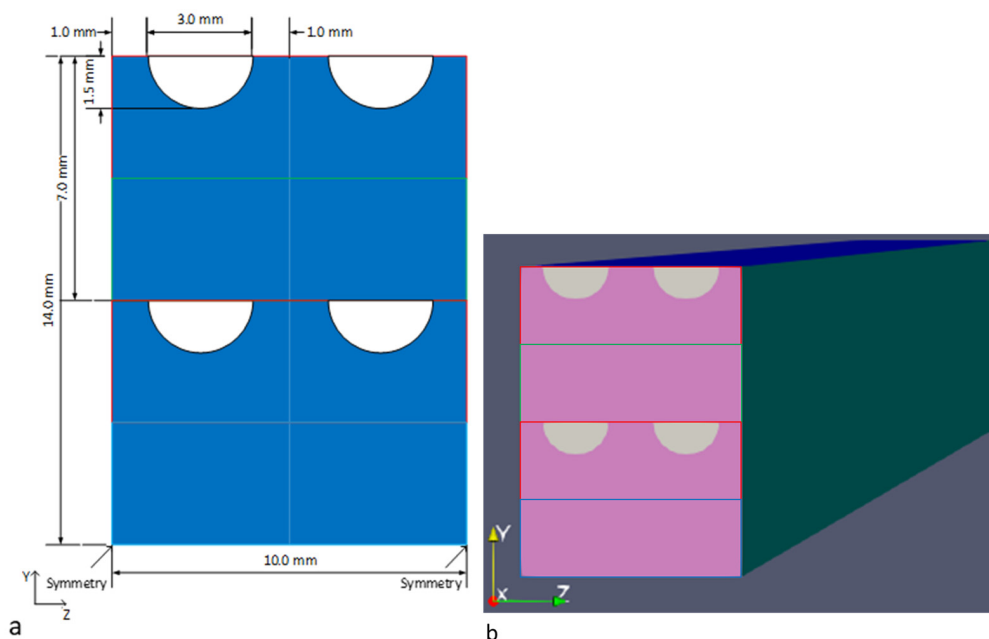


**Figure 4.** Front view of reaction stage modelled geometry consisting of four plates, (a) modelled geometry with dimensions, and (b) 3D OpenFOAM mesh. The direction of flow is into the page along the x-axis. Process plates are enclosed in red, fuel plates in green, and utility plates in blue.

The dimensions of each reaction stage in the y- and z-axes are dictated by the dimensions of the heat transfer section, as they are interconnected. For a scalable section of the reaction stage, the resulting height (14 mm) will be in multiples of the combined thickness of the repeating unit formed by four plates. The reaction stage width is in multiples of the width of a single channel and its wall thickness (i.e., 5 mm).

Considering Figure 4, the modelled PCHE's geometrical parameters and inlet flow conditions (for four channels) are given in Table 2. The species concentrations are based

on typical oxy-fuel combustion flue gas O<sub>2</sub>/CO<sub>2</sub> compositions with other contaminants removed [2]. The stoichiometric amount of fuel needed to achieve the desired O<sub>2</sub> consumption is used. These operating conditions are selected to achieve a Reynolds number of around 8000 in the process flow channels to generate a turbulent flow and enhance post-reaction heat recovery.

**Table 2.** Modelled geometry parameters and inlet flow rate for a single reaction stage, as per Figure 4.

	Value	Unit
Height	14	mm
Width	10	mm
Length	60	mm
Particle diameter	2	mm
Catalyst coating thickness	0.4	mm
Catalyst weight	13.3	g
Packed bed porosity	0.45	-
Process fluid inlet flow rate	7.62	kg/h
Fuel inlet flow rate	0.01	kg/h
Process fluid CO <sub>2</sub> mass fraction (1st stage)	0.978	-
Process fluid inlet O <sub>2</sub> mass fraction (1st stage)	0.022	-
Inlet fluid pressure (1st stage)	1000	kPa
Inlet fluid temperature (1st stage)	500	°C
Axial dispersion coefficient	0.005	m <sup>2</sup> /s

The reaction stages of the PCHE are divided into two categories: the repeating stages and the final stage. As the repeating stages have the same dimensions, only the first repeating stage and the last stage are simulated to obtain temperature and species concentration axial profiles. The inlet conditions in Table 2 are for the first reaction stage, and the subsequent stages' inlet conditions are obtained by global mass and energy balances. The bed length of a given repeating stage consumes the methane fuel, reducing it to a concentration below 0.01 wt%, while the final-stage bed length consumes oxygen to a concentration below 0.007 wt% (100 ppmv). Note that the modeled stage length of 0.06 m is only chosen to achieve a sufficient extent of reaction. The minimum number of reaction stages is five, based on a maximum temperature rise of 50 °C per stage, resulting in a per-stage reduction of 22% of the total O<sub>2</sub> for the four repeating stages.

Considering Figure 4b, the 1D model uses the entire cross-section of the reaction stage as the inlet for the process fluid, while the 3D model only uses the semi-circular inlet ports. The 3D fluid flow field was obtained using OpenFOAM (version 10) [21] with the multiphaseEulerFoam solver, which takes a unity Lewis number assumption. As a result, the process and fuel flows into the reaction stage were pre-mixed for all OpenFOAM simulations.

The multiphaseEulerFoam simulation uses a max time step size of  $1 \times 10^{-4}$  s, with the adjustTimeStep function turned on, and a maxCo of two.

The solver and tolerance, algorithm control, and under-relaxation factors dictated by the fvSolution dictionary are as follows (Table 3).

The discretization schemes dictated in the fvschemes dictionary largely follow the default multiphaseEulerFoam settings, with the laplacianSchemes and snGradSchemes changed to "Gauss linear corrected" and "corrected", respectively. The OpenFOAM mesh is composed of 295,200 cells, with 400 by 35 by 26 cells in the x-, y-, and z-directions, respectively, shared by both the 1D and 3D OpenFOAM models. The 1D ROM mesh is comprised of 120 equal-volume cells along the x-direction.

**Table 3.** Three-dimensional model simulation parameters listed in the fvSolution dictionary.

Attribute	Parameter	Value
solver and tolerance		
nAlphaCorr	alpha.*	1
nAlphaSubCycles	alpha.*	1
solver		
	p_rgh/p_rghFinal	GAMG
	U.*/U.*Final	smoothSolver
	(h e).*/(h e).*Final	smoothSolver
	(Yi).*	PBiCGStab
smoother		
	p_rgh/p_rghFinal	DIC
	U.*/U.*Final	symGaussSeidel
	(h e).*/(h e).*Final	symGaussSeidel
preconditioner		
	(Yi).*	DILU
tolerance		
	p_rgh/p_rghFinal	$1 \times 10^{-7}$
	U.*/U.*Final	$1 \times 10^{-7}$
	(h e).*/(h e).*Final	$1 \times 10^{-7}$
	(Yi).*	$1 \times 10^{-12}$
relative tolerance		
	p_rghFinal	0
	U.*Final	0
	(h e).*Final	0
	(Yi).*	0

### 3.3. Comparison of 1D ROM to 3D Simulations Using the Base Geometry Design and Five Reaction Stages

The results from the 1D ROM (with  $D_{eff} = 0$ ) were compared to the results from the OpenFOAM simulations reduced to a one-dimensional flow (1D OF) in Figure 5a. The temperature and concentration axial profiles are nearly identical, with a stage length difference of 1.7%. The impact of the 3D flow field is also marginal, as shown in Figure 5b. Figure 6 presents the impact of the dispersion coefficient ( $D_{eff} = 0$  and  $0.005 \text{ m}^2/\text{s}$ ) on the axial temperature and concentration profiles in the 1D ROM. The impact was significant when the predicted stage lengths increased from 0.0285 m to 0.031 m after including axial dispersion. Conversely, the gas-phase outlet temperatures decreased from  $552 \text{ }^\circ\text{C}$  to  $550 \text{ }^\circ\text{C}$  with the inclusion of dispersion effects. There were no appreciable differences between the gas- and solid-phase temperatures in steady state; thus, only the gas-phase temperatures are presented.

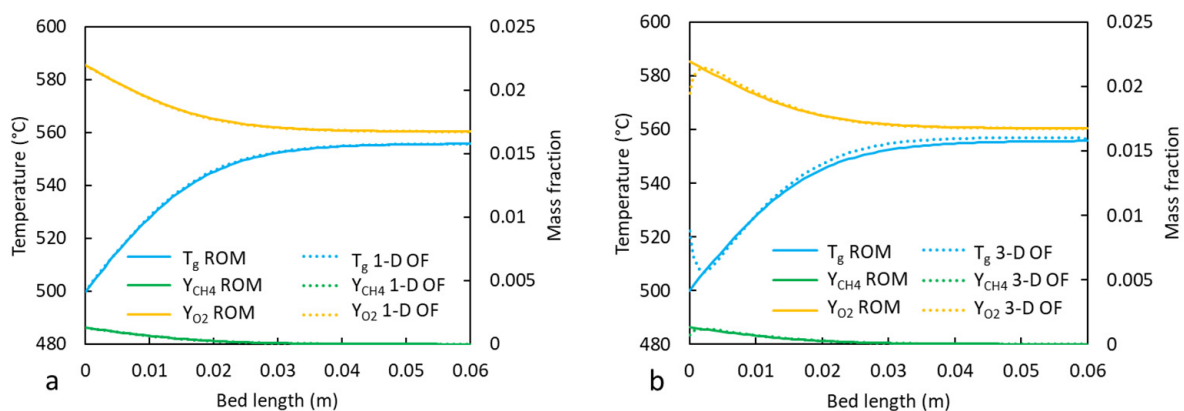


**Figure 5.** Steady-state temperature and species mass fraction profiles for a single reaction stage in a five-stage design: (a) 1D ROM without dispersion vs. 1D OpenFOAM (OF) and (b) 1D ROM without dispersion vs. 3D OF.

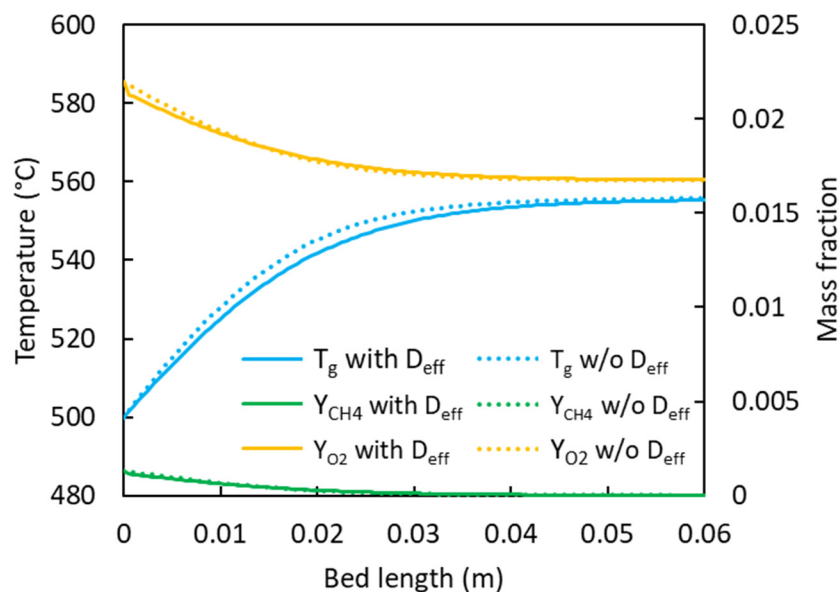


**Figure 6.** Steady-state temperature and species mass fraction profiles for a single reaction stage in a five-stage design with  $D_{eff} = 0.005 \text{ m}^2/\text{s}$  and without axial dispersion.

### 3.4. Impact of the Number of Reaction Stages on PCHE Design

Given that the upper operating temperature is fixed, a lower adiabatic temperature rise (i.e., a higher inlet temperature) will lead to a greater intrinsic rate constant. This is achieved by increasing the number of reaction stages and then adjusting the fuel flow rate and the bed length to reach the target interstage  $\text{CH}_4$  and final-stage  $\text{O}_2$  outlet concentrations. The repeating bed lengths for the PCHE designs with 5 to 11 reaction stages are reported in Table 4. The process fluid inlet conditions and the model geometry are in Table 2. Similarly, the final-stage bed length for each case is reported in Table 5. The cooling capacity in the heat exchanger section before the final stage is reduced to maintain the highest allowed inlet temperature. The total pressure drops from the reaction stages vary from 30.5 to 35.2 kPa for, respectively, the 5- to 11-reaction-stage designs.

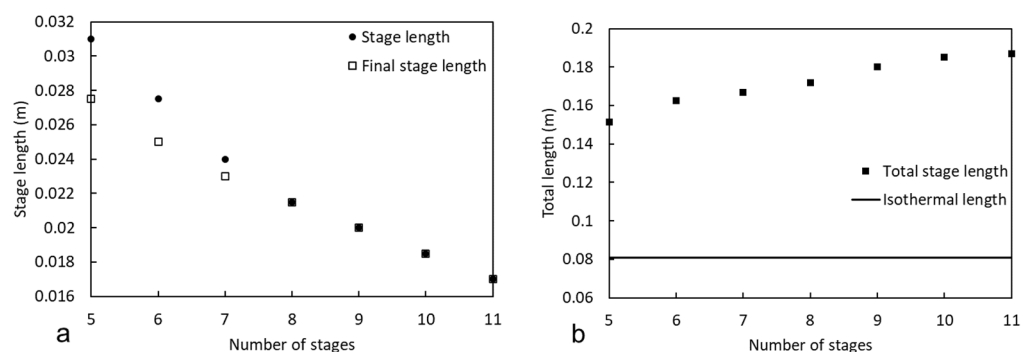
**Table 4.** Simulation results of individual “repeating” stages for PCHE designs with 5 to 11 reaction stages.

Number of Reaction Stages	Fuel Flow Rate per Stage [kg/h]	Inlet Temperature [°C]	Average Temperature [°C]	Stage Length [m]	$-\Delta P$ per Stage [kPa]
5	0.01	500	532	0.031	6.2
6	0.0081	509	534	0.0275	5.4
7	0.0068	517	537	0.024	4.6
8	0.0058	522	539	0.0215	4.1
9	0.0051	525	539	0.02	3.8
10	0.0046	528	540	0.0185	3.5
11	0.0041	531	542	0.017	3.2

Figure 7a compares the individual- and final-stage lengths, while Figure 7b compares the combined total length to an ideal isothermal packed bed of the same height and width operated at 550 °C. The final-reaction-stage length required to reach a target oxygen concentration of  $\leq 100$  ppmv does not significantly differ in length from each individual repeating stage, and both approach the same length as the number of total stages exceeds seven for the conditions described.

**Table 5.** Simulation results of “final” stage for PCHE designs with 5 to 11 reaction stages.

Number of Reaction Stages	Fuel Flow Rate [kg/h]	Inlet Temperature [°C]	Average Temperature [°C]	Stage Length [m]	−ΔP[kPa]
5	0.00191	540	547	0.0275	5.7
6	0.00153	542	547	0.025	5.1
7	0.00129	543	547	0.023	4.7
8	0.00111	544	547	0.0215	4.4
9	0.00097	545	548	0.02	4.1
10	0.00087	546	548	0.0185	3.8
11	0.00078	546	548	0.017	3.5

**Figure 7.** (a) Length of individual stages and final stage; (b) total length of all stages compared to length of the ideal isothermal packed bed.

Although the individual bed length decreases as the number of reaction stages increases, the total bed length increases. This can be attributed to the decreased concentration of  $\text{CH}_4$  used to convert a lower amount of oxygen in each stage. As the reaction kinetics are pseudo-first-order with respect to  $\text{CH}_4$ , decreasing its already low concentration reduces the rate of the reaction. Although the inlet temperature increases by as much as  $31\text{ }^\circ\text{C}$  as the number of stages increases, the integrated average temperature within the reaction stage rises by only  $10\text{ }^\circ\text{C}$ . Considering the rate law parameters and process constraints, the optimal multi-packed bed design should thus utilize the least number of reaction stages.

### 3.5. Heat Exchanger Design for the Multi-Stage Packed Bed Designs

The material chosen for the heat exchange section is 316 stainless steel. A two-pass counter-current crossflow pattern is selected for the utility plate (see Figure 1). Although PCHEs can use other flow channel designs, such as zigzag and serpentine, to increase heat transfer performance, these patterns generally have higher pressure drops and fabrication costs. Straight channels were ultimately used in this design for their relatively lower frictional pressure drop.

The heat exchange section is modelled using a thermal circuit approach [22] and uses the Gnielinski correlation [23] for a conservative estimate of the convective heat transfer coefficient. The process fluid enters the heat exchange section at  $\text{Re} = 8000$ , and the utility fluid flow enters at  $\text{Re} = 23,400\text{--}26,700$ , depending on the number of reaction stages. Each heat exchange section is modelled as a single complete unit of a PCHE, which consists of five plates ordered in the  $y$ -axis as utility, process, fuel, process, and utility. Each heat exchange section has a base unit width of  $0.3\text{ m}$ , resulting in a utility channel length of  $0.3\text{ m}$  and 60 process channels in each section. The utility fluid enters as saturated steam at  $10\text{ bar}$  ( $181\text{ }^\circ\text{C}$ ), and the superheat rise is again limited to  $50\text{ }^\circ\text{C}$  to reduce the thermal stress on the PCHE plates. The heat exchange sections are separated into repeating sections between reaction stages and a final section before the final reaction stage. The process channel lengths are designed to reach an integer number of utility channels because the

number of utility channels governs the resulting lengths of the process channels. Details of the heat exchange section modelling results are given in Table 6.

**Table 6.** Heat exchange section model results for PCHE designs with 5 to 11 reaction stages.

Number of Reaction Stages		5	6	7	8	9	10	11
Steam flow rate [kg/h]	Repeating section	71.36	55.97	46.22	39.24	33.64	29.47	25.29
	Final section	15.42	9.86	9.78	8.43	5.65	5.65	4.22
Number of utility channels	Repeating section	29	21	17	14	12	11	9
	Final section	6	4	4	3	2	2	2
Length of utility channels [m]					0.3			
Number of process channels					60			
Length of process channels [m]	Repeating section	0.29	0.21	0.17	0.14	0.12	0.11	0.09
	Final section	0.06	0.04	0.04	0.03	0.02	0.02	0.02
Total length of process channels [m]		0.93	0.88	0.89	0.87	0.86	0.9	0.83
Total $\Delta P$ from process channels [kPa]		29.6	28.1	28.6	28.1	27.8	29.2	27.0

The variation in the total length of the heat exchange sections with the number of packed beds is minimal, as the total energy removed (heat from combustion from deoxygenation) from the gas is the same for all designs. Differences occur due to using an integer number of utility channels (i.e., some designs have more utility channels than required).

Considering Tables 3–5, the PCHE total length and pressure loss are 1.0932 m and 60.1 kPa and 1.0412 m and 62.2 kPa for the 5- and 11-reaction-stage designs. The PCHE total length is governed by the heat exchanger sections, whereas the pressure drops through the packed beds are greater than through the heat exchanger sections. The maximum total pressure drop for the PCHE design was 6.4% of the inlet pressure.

#### 4. Conclusions

To remove residual oxygen from oxy-fuel combustion flue gases, an intensified heat exchange reactor for catalytic methane combustion is designed based on a printed circuit heat exchanger embedded with multiple adiabatic packed beds. A transient one-dimensional flow model of the packed bed reactor was implemented in Python with Cantera as the reaction solver, and the results were compared to OpenFOAM CFD 3D modelling. The impact of multi-dimensional effects was marginal on the temperature and concentration axial profiles due to the PCHE geometrical design. However, axial dispersion significantly impacts gas-phase mixing and leads to greater bed masses to achieve the required level of deoxygenation.

Design cases for 5 to 11 adiabatic packed bed reaction stages were created using consistent fluid flow and catalyst properties constrained by the criteria of a maximum adiabatic temperature rise of 50 °C and a 10% pressure loss. Each case was evaluated by determining the repeating-reaction-stage length to reduce the fuel concentration to 0.01 wt% and the final-stage length to reduce the O<sub>2</sub> concentration to 0.007 wt% (100 ppmv). More reaction stages naturally shorten the individual stage lengths but ultimately increase the reactor's total bed length due to the impact of reducing the methane concentration being greater than that of a rise in temperature on the reaction rate.

The post-reaction heat exchange sections were designed using a thermal circuit approach, with the results showing similar combined heat exchanger lengths for all cases. The final PCHE design uses five reaction stages at a total length of 1.09 m and a processing rate of 12.3 kg/s flue gas per m<sup>3</sup> PCHE.

**Author Contributions:** Conceptualization, H.G., A.J.F., S.C., R.W.H., J.B.H. and A.M.; formal analysis, H.G. and A.J.F.; funding acquisition, S.C., R.W.H., J.B.H. and A.M.; investigation, H.G. and A.J.F.; methodology, H.G., J.B.H. and A.M.; project administration, S.C., R.W.H., J.B.H. and A.M.; software, H.G. and A.J.F.; supervision, S.C., R.W.H., J.B.H. and A.M.; visualization, H.G.; writing—original draft, H.G.; writing—review and editing, A.J.F., S.C., R.W.H., J.B.H. and A.M. All authors have read and agreed to the published version of the manuscript.

**Funding:** This research was funded by the Program for Energy Research and Development (PERD) at Natural Resources Canada, Government of Canada.

**Data Availability Statement:** Dataset available on request from the authors.

**Acknowledgments:** The authors would like gratefully acknowledge the support provided by the Natural Sciences and Engineering Research Council of Canada (NSERC) and the support and resources were provided by the Digital Research Alliance of Canada (<https://alliancecan.ca/> accessed on 1 October 2023).

**Conflicts of Interest:** The authors declare no conflict of interest.

## Nomenclature

$a_c$	Specific surface area of the particle [ $\text{m}^2/\text{m}^3$ ]
$c_g$	Gas specific heat capacity [ $\text{J}/(\text{kg}\cdot\text{K})$ ]
$d_h$	Flow channel hydraulic diameter [m]
$d_{sv}$	Sauter mean diameter of the particle [m]
$h$	Convective heat transfer coefficient [ $\text{W}/(\text{m}^2\cdot\text{K})$ ]
$k$	Thermal conductivity [ $\text{W}/(\text{m}\cdot\text{K})$ ]
$k_m$	Mass transfer coefficient [m/s]
$\dot{m}$	Mass flow rate [kg/s]
$q_R$	Heat of reaction [ $\text{W}/\text{m}^3$ ]
$t$	Time [s]
$u$	Superficial velocity [m/s]
$A_c$	Cross-sectional area of flow channel [ $\text{m}^2$ ]
$D$	Mass diffusivity [ $\text{m}^2/\text{s}$ ]
$D_{\text{eff}}$	Axial dispersion coefficient [ $\text{m}^2/\text{s}$ ]
$P$	Pressure [Pa]
$H$	Enthalpy [J/kg]
$Pr$	Prandtl number = $c_g\mu_g/k_g$ [-]
$R$	Rate of reaction [1/s]
$Re$	Reynolds number in the flow channel = $\rho_g d_h u_g / \mu_g$ [-]
$Re_p$	Reynolds number in the packed bed = $\rho_g d_{sv} u_g / \epsilon \mu_g$ [-]
$Nu$	Nusselt number in packed bed = $h_g d_{sv} / k_g$ [-]
$Sc$	Schmidt number = $\mu_g / D \rho_g$ [-]
$Sh$	Sherwood number in packed bed = $k_m d_{sv} / D$ [-]
$T$	Temperature [K]
$Y$	Mass fraction [-]
$\epsilon$	Bed void fraction [-]
$\mu$	Dynamic viscosity [Pa·s]
$\rho$	Density [ $\text{kg}/\text{m}^3$ ]
Subscripts	
$g$	Gas phase
$s$	Solid phase

## References

- Zhang, Y.; Xie, Y.; Zhu, Y.; Lu, X.; Ji, X. Energy consumption analysis for CO<sub>2</sub> separation from gas mixtures with liquid absorbents. *Energy Procedia* **2014**, *61*, 2695–2698. [[CrossRef](#)]
- Zheng, L. *Oxy-Fuel Combustion for Power Generation and Carbon Dioxide (CO<sub>2</sub>) Capture*; Woodhead Pub: Philadelphia, PA, USA, 2011.
- Hetland, J. Flue gas processing: Strategies for water management. Water removal and moisture control via dew point modelling. In Proceedings of the IEA Greenhouse Gas R & D Programme (leaghg), Ponferrada, Spain, 9–13 September 2013.
- de Visser, E.; Hendriks, C. *DYNAMIS CO<sub>2</sub> Quality Recommendations*; DYNAMIS Consortium: Brussels, Belgium, 2007.

5. Isothermal Reactor. Linde Engineering. Available online: [https://www.linde-engineering.com/en/process-plants/hydrogen\\_and\\_synthesis\\_gas\\_plants/gas\\_generation/isothermal\\_reactor/index.html#:~:text=The%20Linde%20isothermal%20reactor%20is,of%20a%20straight%20tube%20reactor](https://www.linde-engineering.com/en/process-plants/hydrogen_and_synthesis_gas_plants/gas_generation/isothermal_reactor/index.html#:~:text=The%20Linde%20isothermal%20reactor%20is,of%20a%20straight%20tube%20reactor) (accessed on 12 December 2023).
6. Turton, R.; Shaeiwitz, J.A. *Chemical Process Equipment Design*; Prentice Hall: Boston, MA, USA, 2017.
7. Anxionnaz, Z.; Cabassud, M.; Gourdon, C.; Tochon, P. Heat exchanger/reactors (HEX reactors): Concepts, technologies: State-of-the-art. *Chem. Eng. Process.* **2008**, *47*, 2029–2050. [[CrossRef](#)]
8. Heat Exchangers for Chemical Processing Industries. Available online: <https://www.heatric.com/heat-exchangers/industry-applications/chemical-processing-industry/> (accessed on 3 July 2023).
9. Characteristics of Diffusion-Bonded Heat Exchangers. Available online: <https://www.heatric.com/heat-exchangers/features/characteristics/> (accessed on 1 March 2024).
10. Chung, S.; Lee, S.W.; Kim, N.; Shin, S.M.; Kim, M.H.; Jo, H. Experimental study of printed-circuit heat exchangers with airfoil and straight channels for optimized recuperators in nitrogen Brayton cycle. *Appl. Therm. Eng.* **2023**, *218*, 119348. [[CrossRef](#)]
11. Wang, Y.; Xie, G. 4E multi-objective optimization of cold electricity co-generation system based on supercritical CO<sub>2</sub> Brayton cycle. *Energy Convers. Manag.* **2023**, *283*, 116952. [[CrossRef](#)]
12. Shin, C.W.; No, H.C. Experimental study for pressure drop and flow instability of two-phase flow in the PCHE-type steam generator for SMRs. *Nucl. Eng. Des.* **2017**, *318*, 109–118. [[CrossRef](#)]
13. Zhang, H.; Shi, L.; Xuan, W.; Chen, T.; Li, Y.; Tian, H.; Shu, G. Analysis of printed circuit heat exchanger (PCHE) potential in exhaust waste heat recovery. *Appl. Therm. Eng.* **2022**, *204*, 117863. [[CrossRef](#)]
14. Haynes, B.S.; Johnston, A.M. Process design and performance of a microstructured convective steam-methane reformer. *Catal. Today* **2011**, *178*, 34–41. [[CrossRef](#)]
15. Banister, J.A.; Rumbold, S.O. A compact gas-to-methanol process and its application to improved oil recovery. In Proceedings of the Gas Processors Association Europe Annual Conference, Warsaw, Poland, 21–23 September 2005.
16. Goodwin, G.; Speth, R.L.; Moffatand, H.K.; Weber, B.W. *Cantera: An Object-Oriented Software Toolkit for Chemical Kinetics, Thermodynamics, and Transport Processes*, Version 2.5.1; Zenodo: Geneva, Switzerland, 2021. Available online: <https://www.cantera.org> (accessed on 1 October 2023). [[CrossRef](#)]
17. Levenspiel, O. *Chemical Reacting Engineering*, 3rd ed.; John Wiley & Sons: New York, NY, USA, 1999.
18. Gunn, D. Transfer of heat or mass to particles in fixed and fluidised beds. *Int. J. Heat Mass Transf.* **1978**, *21*, 467–476. [[CrossRef](#)]
19. Nasr, S.; Semagina, N.; Hayes, R.E. Kinetic Modelling of Co<sub>3</sub>O<sub>4</sub>- and Pd/Co<sub>3</sub>O<sub>4</sub>-Catalyzed Wet Lean Methane Combustion. *Emiss. Control Sci. Technol.* **2020**, *6*, 269–278. [[CrossRef](#)]
20. Shen, J.; Hayes, R.E.; Semagina, N. On the contribution of oxygen from Co<sub>3</sub>O<sub>4</sub> to the Pd-catalyzed methane combustion. *Catal. Today* **2021**, *360*, 435–443. [[CrossRef](#)]
21. OpenFOAM | Free CFD Software | The OpenFOAM Foundation. Available online: <https://openfoam.org/> (accessed on 1 October 2023).
22. Bergman, T.L.; Lavine, A.S.; Incropera, F.P.; Dewitt, D.P. *Fundamentals of Heat and Mass Transfer*, 7th ed.; John Wiley & Sons: Hoboken, NJ, USA, 2011.
23. Gnielinski, V. Neue Gleichungen für den Wärme- und den Stoffübergang in turbulent durchströmten Röhren und Kanälen. *Forsch. Ingenieurwes./Eng. Res.* **1975**, *41*, 8–16. [[CrossRef](#)]

**Disclaimer/Publisher’s Note:** The statements, opinions and data contained in all publications are solely those of the individual author(s) and contributor(s) and not of MDPI and/or the editor(s). MDPI and/or the editor(s) disclaim responsibility for any injury to people or property resulting from any ideas, methods, instructions or products referred to in the content.